Nuclear Engineering and Technology 52 (2020) 1742–1748

Contents lists available at ScienceDirect

Nuclear Engineering and Technology

journal homepage: www.elsevier.com/locate/net

Original Article

Terminal solid solubility of hydrogen of optimized-Zirlo and its effects on hydride reorientation mechanisms under dry storage conditions

Ju-Seong Kim [a], Tae-Hoon Kim [b], Kyung-min Kim [c], Yong-Soo Kim [c, *]

[a] Korea Atomic Energy Research Institute, 989-111 Daedeokdaero, Yuseong-gu, Daejeon, 34057, South Korea
[b] Korea Institute of Nuclear Safety, 62 Gwahak-ro, Yuseong-gu, Daejeon, 34142, South Korea
[c] Hanyang University, 222 Wangsimni-ro, Seongdong-gu, Seoul, 04763, South Korea

ARTICLE INFO

Article history:
Received 20 August 2019
Received in revised form
10 January 2020
Accepted 19 January 2020
Available online 22 January 2020

Keywords:
TSSD of hydrogen
TSSP
And TSSP2
Zirlo™
Hydride reorientation

ABSTRACT

TSSD, TSSP, and TSSP2 of hydrogen for optimized-Zirlo (Zirlo™) alloy were measured by DSC in the range of 53–457 wppm. Solvus curves of the TSSs are derived and proposed in this study. The results show that the temperature gap between TSSD and TSSP solvus lines of Zirlo™ are similar to those of other zirconium alloys, but another gap between the TSSD and TSSP2 line differs significantly. In particular, the TSSP2 solvus line becomes closer to the TSSD solvus line than to TSSP unlike Zircaloy-4, so $\Delta T_{TSSD\text{-}TSSP2}$ of Zirlo™ decreases with decreasing temperature. This implies that hydride reorientation can take place more significantly in Zirlo™ than in Zircaloy-4, and the limited temperature variation of 65 °C during the vacuum drying and the cooling-down process may not be sufficient to prevent the triggering of hydride reorientation in Zirlo™ cladding under long-term dry storage.

1. Introduction

Zirconium (Zr) alloys have been used as a cladding material in water nuclear reactors (LWRs and PHWRs) due to their low neutron absorption cross section and advantageous mechanical properties as well as good corrosion resistance in harsh reactor environments; however, they react with coolant water and pick up hydrogen during waterside corrosion. Consequently, the hydrogen concentration in the cladding is basically proportional to the oxide thickness of the cladding materials. The absorbed hydrogen precipitates into Zr hydrides when the hydrogen concentration exceeds the terminal solid solubility (TSS) of hydrogen in the Zr matrix [1–3]. In actuality, the hydrogen TSS of Zr alloys at room temperature is less than 10 wppm, and therefore most of the hydrogen in the Zr matrix precipitates at room temperature.

The precipitated hydrides lying in the circumferential direction of the cylindrical cladding are called circumferential hydrides whereas the hydrides precipitating perpendicular to the circumferential direction are defined as radial hydrides. Circumferential hydride embedded Zr alloy cladding can endure significant deformation, and most of the hydrides in the cladding precipitates in the circumferential direction while normal operation. In fact, this is the reason that metallurgical texture of the zirconium alloy is controlled during cladding tube manufacturing process.

Since Zr hydrides are extremely brittle especially at low temperatures the hydrides can cause the cladding ductility to deteriorate and induce significant embrittlement if radial hydrides form in the cladding. In fact, the radial hydrides can form in the cladding when higher stress than threshold stress for hydride reorientation (HR) is applied during precipitation [4–6]. In this case, the radial hydride embedded Zr alloy cladding can lose its ductility drastically, even with small hydrogen concentrations [6–9]. The hydride embrittlement and the ductile to brittle transition temperature (DBTT) of the Zr alloys are heavily dependent on the hydrogen concentration and the orientations of the hydrides. Thus, the hydrogen TSS of Zr alloys and hydride reorientation (HR) [5,7,10] as well as delayed hydride cracking (DHC) [11,12] are of principal interest in integrity assessments of spent nuclear fuel (SNF) under long-term dry storage operation [13–15].

Due to the specific volume mismatch [16] between the hydrides and the Zr matrix, hydride precipitation induces tensile stress in the Zr matrix and compressive stress in the hydrides, which leads to solubility hysteresis during heating and cooling, referred to as TSS for dissolution (TSSD) and precipitation (TSSP) [16–18]. TSSD is rather independent of thermal history, whereas TSSP is heavily

* Corresponding author.
E-mail address: yongskim@hanyang.ac.kr (Y.-S. Kim).

https://doi.org/10.1016/j.net.2020.01.022

dependent on the thermal history such as maximum temperature, holding time, and cooling rates [19]. Among these variables, the maximum temperature, i.e., the pre-heating temperature before the beginning of precipitation, has the strongest effect on TSSP. In fact, it has been revealed that there are two types of hydride precipitation solvus lines, TSSP1 and TSSP2 [17,20]. TSSP1 represents the hydride nucleation (hereafter, TSSP1 is referred to as TSSP to avoid confusion) whereas TSSP2 denotes the hydride growth. In other words, TSSP solvi is the points that hydrides begin to precipitate from the state that all the hydrides are dissolved, and TSSP2 solvi is the points that hydrides begin to precipitate from the state that hydride and hydrogen in the Zr matrix have an equilibrium. Interestingly, HR occurs only during cool-down, i.e., when the hydrogen solid solution precipitates in the Zr matrix. Therefore, HR is closely related with TSSPs. Similarly, the DHC arrest and initiation temperatures [21,22] are also closely related with the TSS of hydrogen, though debates over its driving force and mechanisms continue [23–28].

Owing to the hydride degradation mechanisms mentioned above, the TSS of hydrogen has been studied for early developed Zr alloys such as Zircaloy-2, Zircaloy-4, and Zr-2.5Nb using differential scanning calorimetry (DSC) [29–32], dilatometry [18,33], internal friction [17,34], and synchrotron X-ray diffraction (XRD) [35–37]; however, there are few available data [38,39] on advanced Zr alloys containing Nb such as Zirlo®, M5, MDA, and Hana. Thus, in this study, the TSS of hydrogen for Zirlo™ was experimentally investigated using DSC and its effects on the formation of radial hydrides under dry storage conditions were discussed.

2. Experimental

2.1. Materials

In the present TSS measurements, partially recrystallized Zirlo™ (Zr-1.0Nb-0.7sn-0.1Fe) was used. As-received specimens were cleaned and charged with hydrogen at 400 °C by a modified Sieverts apparatus [29]. After hydrogen charging, heat treatment was performed at the same temperature for 10 h to ensure uniform hydride distribution, and then the specimens were slowly cooled down to room temperature at a cooling rate of 0.5–1 °C/min.

2.2. Measurement

Hydrogen TSS of Zirlo™ was measured using a heat flux DSC (Netzsch 200 F3) in a purified N_2 flowing environment with the rate of 50 cm^3/min. To dissolve all hydrides in the Zr matrix, specimens were heated to 580 °C and then cooled down to 50 °C. In the DSC measurement, the heat-up and cool-down rates of 20 °C/min were employed. Detailed procedure for DSC measurement is described in detail in the previous work [29]. The maximum slope temperature (MST) in the DSC curve was taken as the final temperature for hydride dissolution (TSSD) and the onset temperature of hydride precipitation (TSSP) at a given hydrogen concentration. At least four thermal cycles were repeated to determine the TSSD and TSSP temperatures of the specimens. In order to measure the TSSP2, and additional thermal cycles were followed after the determination of dissolution temperature of hydrides in each specimen, and the peak temperature prior to cooling is adjusted to the temperature slightly higher than TSSD temperature because TSSD solvi is the border line between α-Zr and α-Zr+δ-hydrides. The difference between the peak temperature for TSSP2 measurement and TSSD temperature is less than 5 °C. After the DSC measurement, all specimens were cleaned with acetone in an ultrasonic bath and hydrogen concentration measurement was carried out using a LECO RH-404 hydrogen analyzer with an uncertainty of less than 5 wppm. They were found to be in the range of 53–457 wppm.

3. Results and discussion

3.1. Measured hydrogen terminal solid solubility of Zirlo™

As mentioned in the introduction, there are three types of TSS of hydrogen in Zr alloys: one for hydride dissolution (TSSD) and two for hydride precipitation (TSSP and TSSP2). Fig. 1 shows the raw data of the typical DSC curves measured in this study during the heat-up and cool-down of the specimens. Fig. 2 shows the Arrhenius plots of the all measured hydrogen TSS data of Zirlo™ in this study, demonstrating single TSSD and two distinct TSSPs. The best-fitting expressions for the hydrogen TSS data of the alloy in the figure can be expressed as follows:

$$C_{TSSD} = 7.8029 \times 10^4 \exp\left(-32,620/_{RT}\right),$$

$$C_{TSSP} = 2.0663 \times 10^4 \exp\left(-21,937/_{RT}\right),$$

$$C_{TSSP2} = 1.3256 \times 10^5 \exp\left(-32,824/_{RT}\right),$$

where C is the hydrogen concentration in wppm, R is the gas constant (8.314 J/mol), and T is the absolute temperature.

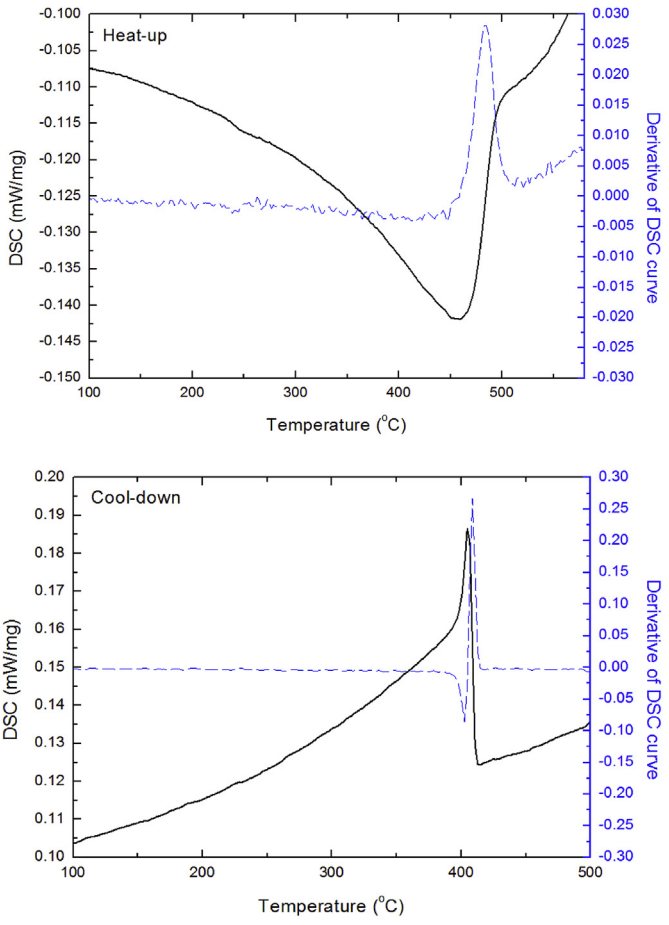

Fig. 1. Typical DSC curve of the phase transition during the heat-up and cool-down of Zirlo™

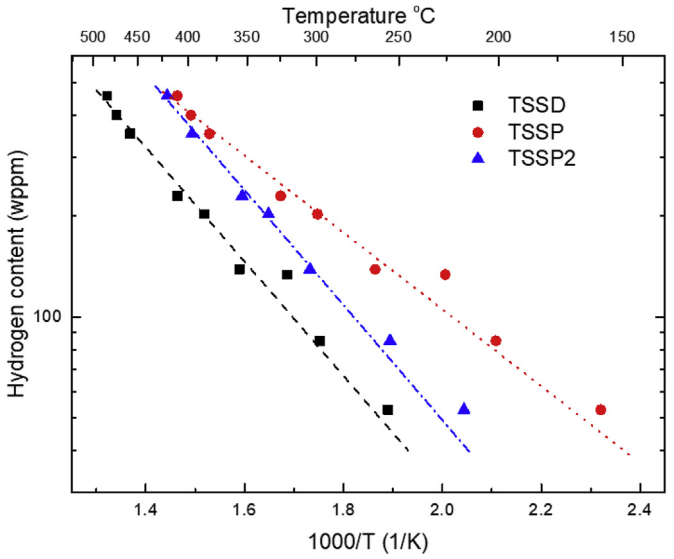

Fig. 2. Measured TSS of the hydrogen of Zirlo™

Fig. 3 shows the hydrogen TSSs of various Zr alloys. Fig. 3a) shows the activation energy of hydride dissolution in Zirlo™, demonstrating that it is in good agreement with other TSSD data ranging in between 30 kJ/mol and 39 kJ/mol taking into consideration that hydrogen TSS depends on measurement techniques [30], data analysis method [20,40], and thermal history [17,29,41,42]. TSSD is close to a thermo-dynamic equilibrium value, and thus the value has little discrepancy.

TSS for the precipitation is close to kinetic value. Fig. 3b) and 3c) reveal that the activation energies of two hydrogen precipitations, i.e., TSSP for hydride nucleation and TSSP2 for hydride growth, are 21.97 kJ/mol and 32.824 kJ/mol, respectively, which seem to be in reasonable agreement given that the TSSP temperature is heavily dependent on the thermal history such as the prior maximum temperature [17], and dwell time at the maximum temperature [19,42]. All the data presented in Fig. 3 are given in Table 1. It is noticeable that the trend of hydrogen TSSP2 of Zirlo™ is quite different from that of Zircaloy-4 [29]. Fig. 4 clearly demonstrates the difference in the hysteresis gap of the hydrogen TSS in both alloys, Zircaloy-4 and Zirlo™. The comparison shows that there is a fairly large gap between TSSD and TSSP2 of hydrogen in Zircaloy-4; in contrast, the gap decreases with decreasing temperature and so the TSSP2 of hydrogen becomes closer to TSSD in Zirlo™. Fig. 5 shows the temperature hysteresis gap between the TSSD and TSSPs ($\Delta T_{TSSD\text{-}TSSPs}$) with regard to the hydride dissolution temperature. The precipitation temperature is dependent on the condition where hydride exists in the Zr matrix when it precipitates. When there is no hydride previously in the Zr matrix, it may be difficult for hydrides to precipitate because specific volume change causes plastic deformation and compressive stress in the surrounding Zr matrix. On the other hand, if there are hydrides already in the Zr matrix, it is easy for hydrides to precipitate or re-precipitate following the former hydrides traces, although elastic strain is inevitably induced during the hydride growth. It has also been reported that precipitation of hydrides in the Zr alloys is closely related to the memory effect [43], that is, dissolved hydrogen tends to re-precipitate at the previous hydride sites. It is quite understood because hydride precipitation possibly accompanies dislocation generation due to the misfit strain [44,45] and the generated dislocation tangles may provide preferential sites for hydride re-precipitation [46,47].

In this respect, $\Delta T_{TSSD\text{-}TSSP2}$ is always smaller than the $\Delta T_{TSSD\text{-}TSSP}$, and all of the data in Fig. 5 demonstrate this trend. However, it is noticeable that the $\Delta T_{TSSD\text{-}TSSP2}$ of Zirlo™ increases with increasing TSSD temperature, and the $\Delta T_{TSSD\text{-}TSSP}$ of Zirlo™ is higher than other Zr alloys. This finding implies that hydride nucleation in the alloy may be more difficult than that in other Zr alloys, while hydrogen could precipitate easily on previous hydrides sites, i.e., hydride growth may be easy when Zirlo™ is subjected to low peak temperature during heat-up. It might be due to the effects of cold-work, alloying elements, grain size or β-Nb distribution although there is no clear evidence yet [1,19,41,48,49]. Another experiment is needed for the identification of the relation between hydride growth, and microstructure of Zr alloys.

3.2. Effects of the TSS of hydrogen on hydride reorientation in Zirlo™ cladding under dry storage conditions

As mentioned earlier, most of observed hydrides in Zr alloy cladding of spent nuclear fuel rods are circumferential because all cladding tubes are treated with a longitudinal cold-rolling process, so-called pilgering process, to control their textures during manufacturing. Interestingly, however, the circumferential hydrides can change their precipitation direction when excessive hoop stress is applied to the cladding during vacuum drying and cooling-down process prior to loading of the spent nuclear fuels to the long-term dry storage cask, which is referred to as HR [6]. Considering hydrogen concentration of spent nuclear cladding and temperature history during dry storage condition, both Zircaloy-4 and Zirlo™ cladding follows the TSSP2 solvi because hydrides will exist when the fuel rod is cooled. Thus the temperature gap between TSSD and TSSP2 is important for understanding HR. Fig. 5 reveals that $\Delta T_{TSSD\text{-}TSSP2}$ of Zirlo™ is smaller than that of Zircaloy-4, which implies that even with identical stress conditions, HR can take place more significantly in Zirlo™ than in Zircaloy-4 with assumptions that all of the variables affecting HR such as texture, residual stress, threshold stress of Zirlo™ and Ziraloy-4 are identical except TSS of Hydrogen. Recent ductility tests of irradiated Zr alloy cladding support that the issue may be more serious in the former than in the latter alloy [8,9]. It was shown that under similar hoop stress and temperature histories, the radial hydride continuity factor (RHCF) of the Zirlo® was larger than that of Zircaloy-4. This difference means that Zirlo® may be more brittle than Zircaloy-4, and consequently the DBTT of the former alloy may be higher than that of the latter [8]. In fact, the ductility of the irradiated Zr cladding can be influenced by many factors such as the irradiation damages, oxide thickness, hydride distribution [50], annealing temperature [9], and alloy texture of Zr. However, it is well-known that the HR is the most critical factor affecting the ductility deterioration of irradiated Zr alloy cladding [8].

In order to minimize the HR in Zr alloy cladding, the U.S. NRC limited the number of thermal cycles to less than 10, and the temperature variation during the repeated thermal cycling to less than 65 °C [51], in addition to the requirement that maximum allowable cladding temperature is 400 °C during long-term dry storage. This guideline is based on the test results of Kammenzind et al. [52] that hydrides rarely precipitate during the temperature gap between the TSSD and TSSP temperatures, i.e., hydride reorientation cannot occur during the temperature hysteresis [5]. However, there are a few recent reports that the temperature hysteresis gap between TSSD and TSSP can be reduced by repeated thermal cycling [53,54], and, furthermore, recent experimental results [29,35] revealed that the hydrogen TSS follows TSSP2, not TSSP, during the hydride precipitation. This means that $\Delta T_{TSSD\text{-}TSSP2}$ is more important than $\Delta T_{TSSD\text{-}TSSP}$ because the peak cladding temperature during dry storage is not high enough to dissolve all

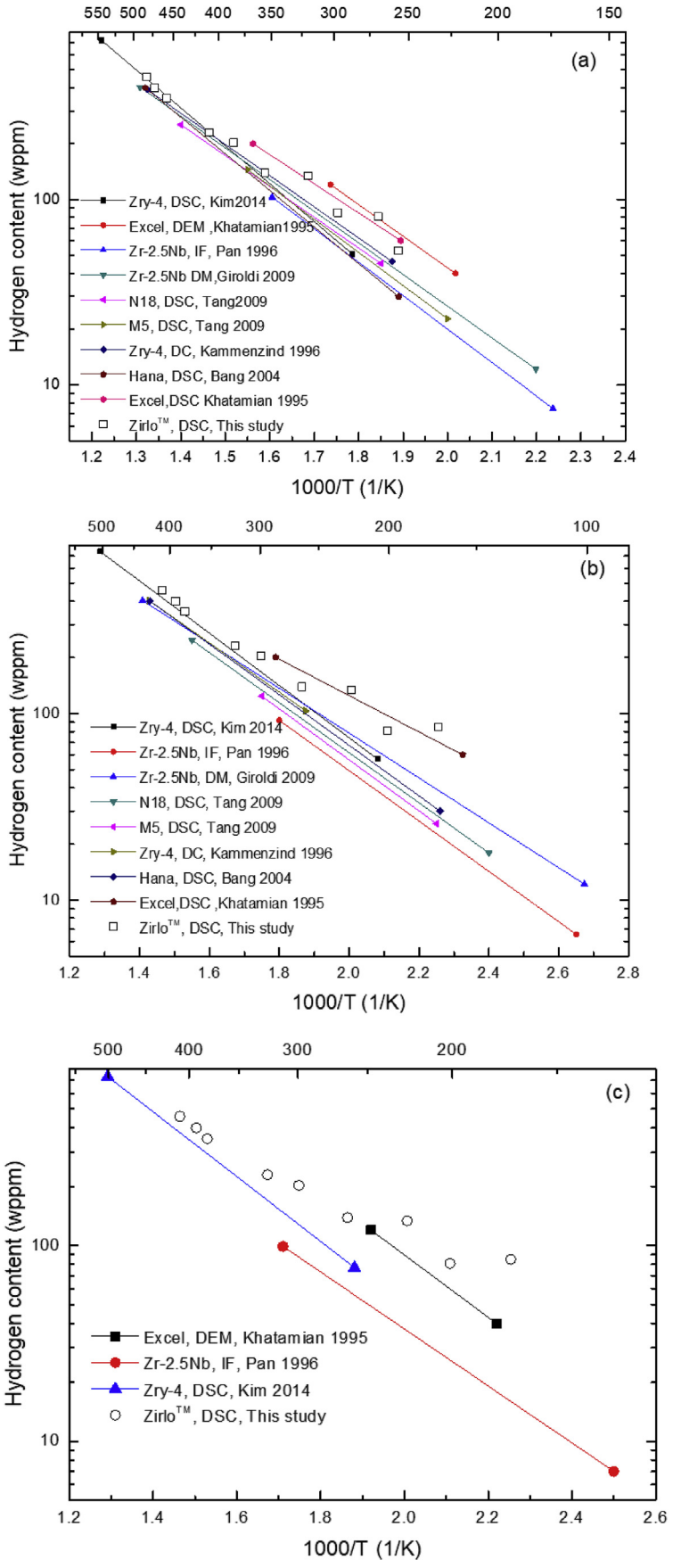

Fig. 3. (a) Comparison of TSSD, (b) TSSP, and (c) TSSP2 of Zirlo™ with those of Zircaloy-4, and other Nb containing Zr alloys

Table 1
Terminal solid solubility of hydrogen in Zr alloys.

TSS	Material	A	Q (kJ/mol)	H content (wppm)	Method	Reference
TSSD	Zircaloy-4	6.6×10^4	32.196	120–450	Diffusion couple (DC)	Kammenzind et al. [52]
	Zircaloy-4	2.255×10^5	39.101	40–731	DSC	Kim et al. [29]
	Zr-2.5Nb	8.08×10^4	34.52	7–99	Internal friction (IF)	Pan et al. [17]
	Zr-2.5Nb	6.11×10^4	31.818	50–463	Dilatometry (DM)	Giroldi et al. [33]
	Excel	1.09×10^5	32.6	40–120	Dynamic elastic modulus (DEM)	Khatamian et al. [30]
		5.72×10^4	30.1	60–200	DSC	
	N18	5.3637×10^4	31.809	20–240	DSC	Tang and Yang [38]
	M5	8.4956×10^4	34.187	20–240		
	Hana-3,5	1.5×10^5	37.424	30–400	DSC	Bang et al. [39]
	Zirlo™	7.8029×10^4	32.62	53–457	DSC	This study
TSSP	Zircaloy-4	3.1×10^4	25.279	120–450	Diffusion couple (DC)	Kammenzind et al. [52]
	Zircaloy-4	4.722×10^4	26.843	40–731	DSC	Kim et al. [29]
	Zr-2.5Nb	2.473×10^4	25.84	7–99	IF	Pan et al. [17]
	Zr-2.5Nb	2.22×10^4	24.618	50–463	DM	Giroldi et al. [33]
	Excel	1.45×10^5	29.9	40–120	DEM	Khatamian et al. [30]
		1.12×10^4	18.7	60–200	DSC	
	N18	2.9732×10^4	25.69	20–240	DSC	Tang and Yang [38]
	M5	3.0368×10^4	26.18	20–240		
	Hana-3 and -5	3.63×10^4	26.133	40–731	DSC	Bang et al. [39]
	Zirlo™	2.0663×10^4	21.973	53–457	DSC	This study
TSSP2	Zircaloy-4	8.612×10^4	30.583	40–731	DSC	Kim et al. [29]
	Excel	1.43×10^5	30.7	40–120	DSC	Khatamian et al. [30]
	Zr-2.5Nb	3.15×10^4	27.99	7–99	IF	Pan et al. [17]
	Zirlo™	1.3256×10^5	32.824	53–457	DSC	This study

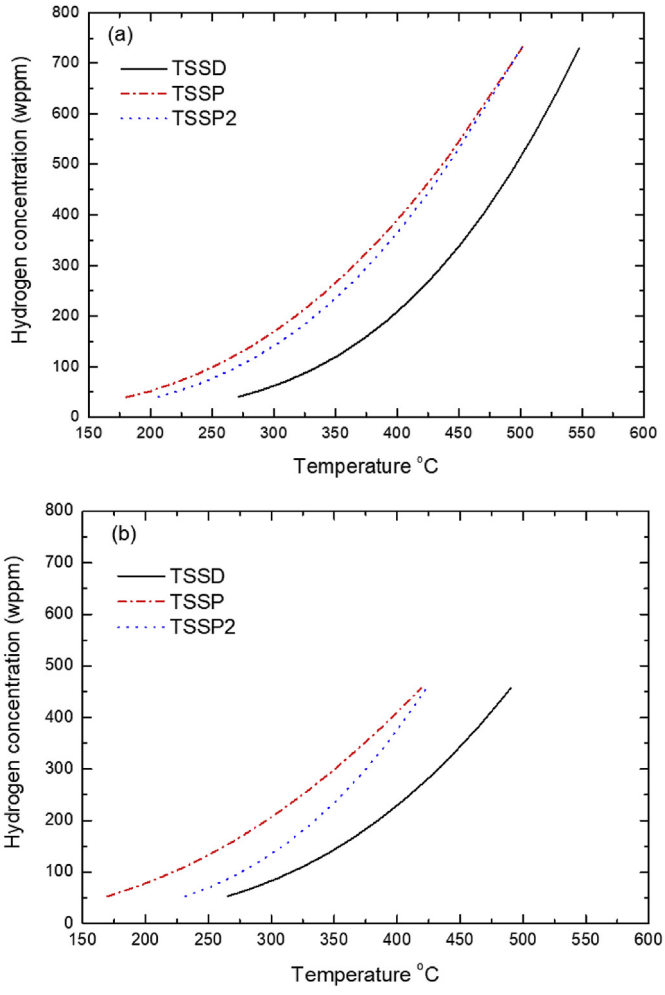

Fig. 4. TSS of H in (a) Zircaloy-4 [29], and (b) ZIRLO™ The curves are based on the best fitting equations of TSS of H in Zirlo™ and Zircaloy-4.

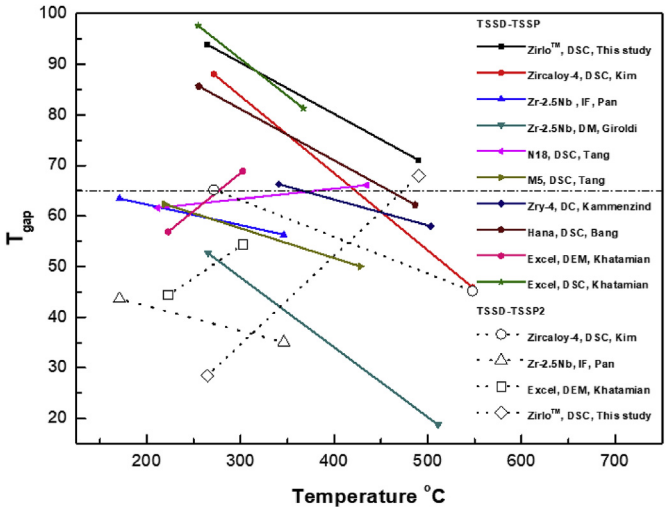

Fig. 5. Temperature variation between the TSSD and TSSPs of Zr alloys

the hydrides in the cladding materials. In this respect, the limited temperature variation of 65 °C during the vacuum drying and cooling-down process may be reasonable and effective to minimize the HR in Zircaloy-4 cladding, given that the maximum allowable cladding temperature remains at 400 °C under long-term dry storage. However, as shown in Fig. 5, the $\Delta T_{TSSD\text{-}TSSP2}$ of Zirlo is less than 65 °C and this probably means that hydride reorientation may occur in this alloy during the thermal cycles, even if the limitation rule is obeyed.

4. Conclusions

TSSD, TSSP, and TSSP2 of hydrogen in Zirlo™ were measured by DSC in the range of 53–457 wppm. Based on the measurement data, the following best-fitting expressions for the solvus curves of the TSSs are derived:

$$C_{TSSD} = 7.8029 \times 10^4 \exp\left(-32,620/_{RT}\right),$$

$$C_{TSSP} = 2.0663 \times 10^4 \exp\left(-21,937/_{RT}\right),$$

$$C_{TSSP2} = 1.3256 \times 10^5 \exp\left(-32,824/_{RT}\right),$$

where C is the hydrogen concentration in wppm, R is the gas constant (8.314 J/mol), and T is the absolute temperature.

The results showed that the TSSD and TSSP temperatures of Zirlo™ are similar to those of other zirconium alloys, and the activation energies for hydride dissolution and precipitation are also in good agreement with those of other Zr alloys. However, the solvus line data of the TSSP2 of the alloy differs remarkably from those of other Zr alloys, particularly Zircaloy-4. The gap in Zirlo™ increases with decreasing temperature, and the TSSP2 solvus line becomes closer to the TSSD solvus line. Though the measurement of TSS of H in this study was not conducted under the stress, this implies that the 65 °C temperature variation limit during the vacuum drying and cooling-down process required for long-term dry storage may not be enough to prevent triggering of hydride reorientation in the spent nuclear fuel rods using Zirlo™ cladding tubes.

Declaration of competing interest

The authors declare that they have no known competing financial interests or personal relationships that could have appeared to influence the work reported in this paper.

Acknowledgements

This work was supported by the Human Resources Program in Energy Technology Korea Institute of Energy Technology Evaluation and Planning(KETEP) and the Ministry of Trade, Industry & Energy(MOTIE) of the Republic of Korea (No. 20184030201970).

Appendix A. Supplementary data

Supplementary data to this article can be found online at https://doi.org/10.1016/j.net.2020.01.022.

References

[1] J.J. Kearns, Terminal solubility and partitioning of hydrogen in the alpha phase of zirconium, Zircaloy-2 and Zircaloy-4, J. Nucl. Mater. 22 (3) (1967) 292–303.
[2] A. Sawatzky, The diffusion and solubility of hydrogen in the alpha phase of zircaloy-2, J. Nucl. Mater. 2 (1) (1960) 62–68.
[3] W.H. Erickson, D. Hardie, The influence of alloying elements on the terminal solubility of hydrogen in α-zirconium, J. Nucl. Mater. 13 (2) (1964) 254–262.
[4] H.C. Chu, S.K. Wu, R.C. Kuo, Hydride reorientation in Zircaloy-4 cladding, J. Nucl. Mater. 373 (1–3) (2008) 319–327.
[5] J.-S. Kim, Y.-J. Kim, D.-H. Kook, Y.-S. Kim, A study on hydride reorientation of Zircaloy-4 cladding tube under stress, J. Nucl. Mater. 456 (2015) 246–252, 0.
[6] J.-S. Kim, T.-H. Kim, D.-H. Kook, Y.-S. Kim, Effects of hydride morphology on the embrittlement of Zircaloy-4 cladding, J. Nucl. Mater. 456 (2015) 235–245, 0.
[7] Y.-J. Kim, D.-H. Kook, T.-H. Kim, J.-S. Kim, Stress and temperature-dependent hydride reorientation of Zircaloy-4 cladding and its effect on the ductility degradation, J. Nucl. Sci. Technol. 52 (5) (2015) 717–727.
[8] M.C. Billone, T.A. Burtseva, R.E. Einziger, Ductile-to-brittle transition temperature for high-burnup cladding alloys exposed to simulated drying-storage conditions, J. Nucl. Mater. 433 (1–3) (2013) 431–448.
[9] M. Aomi, T. Baba, T. Miyashita, K. Kamimura, T. Yasuda, Y. Shinohara, T. Takeda, Evaluation of Hydride Reorientation Behavior and Mechanical Properties for High-Burnup Fuel-Cladding Tubes in Interim Dry Storage, vol. 1505, ASTM special technical publication, 2009, pp. 651–673.
[10] H.-J. Cha, K.-N. Jang, J.-H. An, K.-T. Kim, The effect of hydrogen and oxygen contents on hydride reorientations of zirconium alloy cladding tubes, Nucl. Eng. Technol 47 (6) (2015) 746–755.
[11] C. Coleman, V. Inozemtsev, V. markelov, R. Roth, A.-M. Alvare-Holston, L. Ramanathan, Z. He, J.K. Chakravartty, V. Makarevicius, L. Ali, The threshold stress-intensity factor, K_{IH}, for delayed hydride cracking (DHC) in zircaloy-4 fuel cladding- an IAEA coordinated research project (CRP), in: Proceeding of Water Reactor Fuel Performance Meeting 2014 Sendai, Japan, 2014. Sept 14-17,2014, Paper No. 100048.
[12] A.-M. Alvarez Holston, J. Stjärnsäter, On the effect of temperature on the threshold stress intensity factor of delayed hydride cracking in light water reactor fuel cladding, Nucl. Eng. Technol 49 (4) (2017) 663–667.
[13] Y.S. Kim, Delayed hydride cracking of spent fuel rods in dry storage, J. Nucl. Mater. 378 (1) (2008) 30–34.
[14] K.S. Chan, An assessment of delayed hydride cracking in zirconium alloy cladding tubes under stress transients, Int. Mater. Rev. 58 (6) (2013) 349–373.
[15] J.-S. Kim, J.-D. Hong, Y.-S. Yang, D.-H. Kook, Rod internal pressure of spent nuclear fuel and its effects on cladding degradation during dry storage, J. Nucl. Mater. 492 (2017) 253–259.
[16] M.P. Puls, The effects of misfit and external stresses on terminal solid solubility in hydride-forming metals, Acta Metall. 29 (12) (1981) 1961–1968.
[17] Z.L. Pan, I.G. Ritchie, M.P. Puls, The terminal solid solubility of hydrogen and deuterium in Zr-2.5Nb alloys, J. Nucl. Mater. 228 (2) (1996) 227–237.
[18] G.F. Slattery, The terminal solubility of hydrogen in the zirconium/2 at % chromium/0.16 at % iron alloy, J. Nucl. Mater. 32 (1) (1969) 30–38.
[19] A. McMinn, E.C. Darby, J.S. Schofield, Terminal Solid Solubility of Hydrogen in Zirconium Alloys, vol. 1354, ASTM special technical publication, 2000, pp. 173–195.
[20] Z.L. Pan, M.P. Puls, Precipitation and dissolution peaks of hydride in Zr–2.5Nb during quasistatic thermal cycles, J. Alloys Compd. 310 (1–2) (2000) 214–218.
[21] Y. Kim, S. Choi, Y. Cheong, Review of the initiation and arrest temperatures for delayed hydride cracking in zirconium alloys, Met. Mater. Int. 11 (1) (2005) 39–47.
[22] S.Q. Shi, G.K. Shek, M.P. Puls, Hydrogen concentration limit and critical temperatures for delayed hydride cracking in zirconium alloys, J. Nucl. Mater. 218 (2) (1995) 189–201.
[23] M.P. Puls, Review of the thermodynamic basis for models of delayed hydride cracking rate in zirconium alloys, J. Nucl. Mater. 393 (2) (2009) 350–367.
[24] M.P. Puls, Comments on author's reply to "Review of the thermodynamic basis for models of delayed hydride cracking rate in zirconium alloys", M.P. Puls in J. Nucl. Mater. 393 (2009) 350–367, J. Nucl. Mater. 399 (2–3) (2010) 248–258.
[25] Y.S. Kim, Author's reply to "Review of the thermodynamic basis for models of delayed hydride cracking rate in zirconium alloys, M.P. Puls in J. Nucl. Mater. 393 (2009) 350–367", J. Nucl. Mater. 399 (2–3) (2010) 240–247.
[26] Y.S. Kim, Author's 2nd reply to comments on author's reply to "Review of the thermodynamic basis for models of delayed hydride cracking rate in zirconium alloys," M.P. Puls in J. Nucl. Mater. 393 (2009) 350–367, J. Nucl. Mater. 399 (2–3) (2010) 259–265.
[27] Y.S. Kim, Comments on the Dutton–Puls model: temperature and yield stress dependences of crack growth rate in zirconium alloys, Mater. Sci. Eng., A 527 (29–30) (2010) 7480–7483.
[28] G.A. McRae, C.E. Coleman, B.W. Leitch, The first step for delayed hydride cracking in zirconium alloys, J. Nucl. Mater. 396 (1) (2010) 130–143.
[29] J.-S. Kim, Y.-S. Kim, Effect of thermal history on the terminal solid solubility of hydrogen in Zircaloy-4, Int. J. Hydrogen Energy 39 (29) (2014) 16442–16449.
[30] D. Khatamian, Z.L. Pan, M.P. Puls, C.D. Cann, Hydrogen solubility limits in Excel, an experimental zirconium-based alloy, J. Alloys Compd. 231 (1–2) (1995) 488–493.
[31] K. Une, S. Ishimoto, Dissolution and precipitation behavior of hydrides in Zircaloy-2 and high Fe Zircaloy, J. Nucl. Mater. 322 (1) (2003) 66–72.
[32] K. Une, S. Ishimoto, Terminal solid solubility of hydrogen in unalloyed zirconium by differential scanning calorimetry, J. Nucl. Sci. Technol. 41 (9) (2004) 949–952.
[33] J.P. Giroldi, P. Vizcaíno, A.V. Flores, A.D. Banchik, Hydrogen terminal solid solubility determinations in Zr–2.5Nb pressure tube microstructure in an extended concentration range, J. Alloys Compd. 474 (1–2) (2009) 140–146.
[34] I.G. Ritchie, Z.L. Pan, Internal friction and young's modulus measurements in Zr-2.5Nb alloy doped with hydrogen, ASTM Spec. Tech. Publ. 1169 (1992) 385–395.
[35] O. Zanellato, M. Preuss, J.Y. Buffiere, F. Ribeiro, A. Steuwer, J. Desquines, J. Andrieux, B. Krebs, Synchrotron diffraction study of dissolution and precipitation kinetics of hydrides in Zircaloy-4, J. Nucl. Mater. 420 (1–3) (2012) 537–547.
[36] K.B. Colas, A.T. Motta, M.R. Daymond, J.D. Almer, Effect of thermo-mechanical cycling on zirconium hydride reorientation studied in situ with synchrotron X-ray diffraction, J. Nucl. Mater. 440 (1–3) (2013) 586–595.
[37] O.F. Courty, A.T. Motta, C.J. Piotrowski, J.D. Almer, Hydride precipitation kinetics in Zircaloy-4 studied using synchrotron X-ray diffraction, J. Nucl. Mater. 461 (2015) 180–185, 0.
[38] R. Tang, X. Yang, Dissolution and precipitation behaviors of hydrides in N18, Zry-4 and M5 alloys, Int. J. Hydrogen Energy 34 (17) (2009) 7269–7274.
[39] J.G. Bang, J.H. Baek, Y.H. Jeong, P07G24 determination of terminal solid solubility of hydrogen in zirconium alloys, Korean Nuclear Society 2004 (2004) 1028–1032.
[40] D. Khatamian, DSC "peak temperature" versus "maximum slope temperature" in determining TSSD temperature, J. Nucl. Mater. 405 (2) (2010) 171–176.
[41] D. Khatamian, Effect of β-Zr decomposition on the solubility limits for H in

Zr–2.5Nb, J. Alloys Compd. 356–357 (2003) 22–26.
[42] S.A. Parodi, L.M.E. Ponzoni, M.E. De Las Heras, J.I. Mieza, G. Domizzi, Study of variables that affect hydrogen solubility in α + β Zr-alloys, J. Nucl. Mater. 477 (2016) 305–317.
[43] D.J. Cameron, R.G. Duncan, On the existence of a memoty effect in hydride precipitation in cold-worked Zr-2.5% Nb, J. Nucl. Mater. 68 (3) (1977) 340–344.
[44] G.J.C. Carpenter, The dilatational misfit of zirconium hydrides precipitated in zirconium, J. Nucl. Mater. 48 (3) (1973) 264–266.
[45] G.J.C. Carpenter, J.F. Watters, R.W. Gilbert, Dislocations generated by zirconium hydride precipitates in zirconium and some of its alloys, J. Nucl. Mater. 48 (3) (1973) 267–276.
[46] G.J.C. Carpenter, J.F. Watters, An in-situ study of the dissolution of γ-zirconium hydride in zirconium, J. Nucl. Mater. 73 (2) (1978) 190–197.
[47] J.-S. Kim, S.-D. Kim, J. Yoon, Hydride formation on deformation twin in zirconium alloy, J. Nucl. Mater. 482 (2016) 88–92.
[48] G.F. Slattery, The terminal solubility of hydrogen in zirconium alloys between 30 and 400 °C, J. Inst. Met. 95 (1967) 43–47.
[49] M. Ito, K. Ko, H. Muta, M. Uno, S. Yamanaka, Effect of Nb addition on the terminal solid solubility of hydrogen for Zr and Zircaloy-4, J. Alloys Compd. 446–447 (2007) 451–454.
[50] M.C. Billone, T.A. Burtseva, Effects of Lower Drying-Storage Temperature on the Ductility of High-Burnup PWR Cladding, Argonne National Lab. (ANL), Argonne, IL (United States), 2016, pp. 1–94.
[51] U.S. Nuclear Regulatory Commission (NRC), Interim Staff Guidance-11, 2003. Revision 3.
[52] B.G. Kammenzind, D.G. Franklin, H.R. Peters, W.J. Duffin, Hydrogen Pickup and Redistribution in Alpha-Annealed Zircaloy-4, vol. 1295, ASTM special technical publication, 1996, pp. 338–369.
[53] H.E. Weekes, N.G. Jones, T.C. Lindley, D. Dye, Hydride reorientation in Zircaloy-4 examined by in situ synchrotron X-ray diffraction, J. Nucl. Mater. 478 (2016) 32–41.
[54] P. Vizcaíno, J.R. Santisteban, M.A. Vicente Alvarez, A.D. Banchik, J. Almer, Effect of crystallite orientation and external stress on hydride precipitation and dissolution in Zr2.5%Nb, J. Nucl. Mater. 447 (1–3) (2014) 82–93.